Article

Structure

Structural Impact of Tau Phosphorylation at Threonine 231

Graphical Abstract

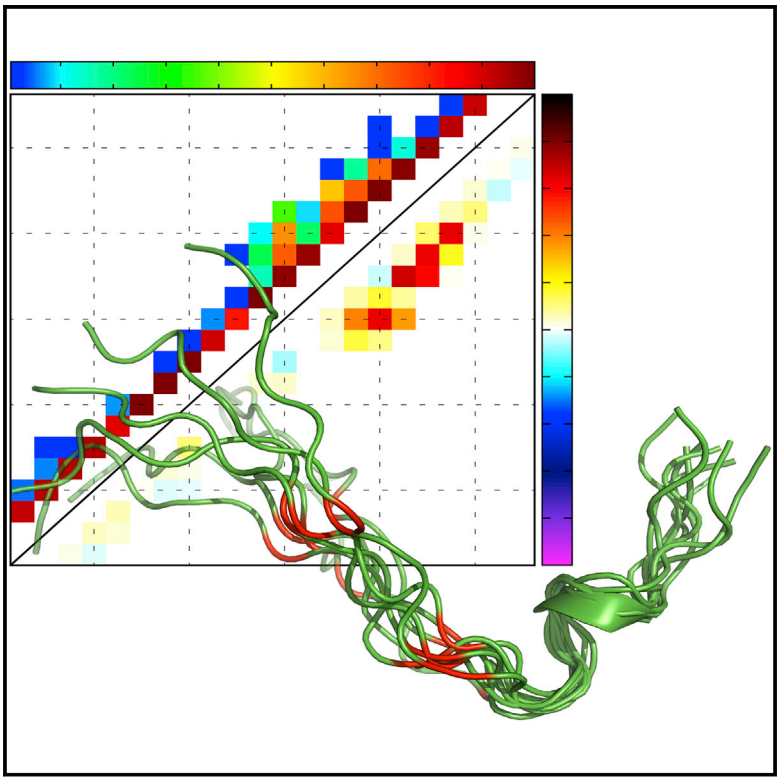

Authors

Martin Schwalbe,
Harindranath Kadavath,
Jacek Biernat, ..., Martin Blackledge,
Eckhard Mandelkow,
Markus Zweckstetter

Correspondence

markus.zweckstetter@dzne.de

In Brief

Alzheimer disease-related protein Tau is a phosphoprotein, and a number of different residues are subject to phosphorylation. Schwalbe et al. develop a molecular ensemble approach and use it to reveal an atomic-level description of the phosphorylation-induced structural changes in Tau phosphorylated at Thr231.

Highlights

- A novel ensemble calculation approach was developed
- Molecular ensembles of phosphorylated Tau fragments were determined
- Phosphorylated T231 selectively engages in a salt bridge with R230
- Integration of NOE restraints with ensemble calculations are highly useful for IDPs

Schwalbe et al., 2015, Structure *23*, 1448–1458
August 4, 2015
http://dx.doi.org/10.1016/j.str.2015.06.002

CellPress

Structure
Article

Structural Impact of Tau Phosphorylation at Threonine 231

Martin Schwalbe,[1] Harindranath Kadavath,[1,2] Jacek Biernat,[3] Valery Ozenne,[4] Martin Blackledge,[4] Eckhard Mandelkow,[3,5] and Markus Zweckstetter[1,2,6,*]

[1]German Center for Neurodegenerative Diseases (DZNE), 37077 Göttingen, Germany
[2]Department for NMR-based Structural Biology, Max Planck Institute for Biophysical Chemistry, 37077 Göttingen, Germany
[3]German Center for Neurodegenerative Diseases (DZNE), 53175 Bonn, Germany
[4]Institut de Biologie Structurale Jean-Pierre Ebel, CEA-CNRS-UJF UMR 5075, 41 Rue Jules Horowitz, Grenoble 38027, France
[5]CAESAR Research Center, Ludwig-Erhard-Allee 2, 53175 Bonn, Germany
[6]DFG Research Center for Nanoscale Microscopy and Molecular Physiology of the Brain (CNMPB), University Medical Center Göttingen, 37073 Göttingen, Germany
*Correspondence: markus.zweckstetter@dzne.de
http://dx.doi.org/10.1016/j.str.2015.06.002

SUMMARY

Phosphorylation of the microtubule-associated protein Tau influences the assembly and stabilization of microtubules and is deregulated in several neurodegenerative diseases. The high flexibility of Tau, however, has prevented an atomic-level description of its phosphorylation-induced structural changes. Employing an extensive set of distance and orientational restraints together with a novel ensemble calculation approach, we determined conformational ensembles of Tau fragments in the non-phosphorylated state and, when phosphorylated at T231/S235 or T231/S235/S237/S238, four important sites of phosphorylation in Alzheimer disease. Comparison of the molecular ensembles showed that phosphorylation of the regulatory T231 does not perturb the backbone conformation of the proximal microtubule-binding ^{225}KVAVVR^{230} motif. Instead, phosphorylated T231 selectively engages in a salt bridge with R230 that can compete with the formation of intermolecular salt bridges to tubulin. Our study provides an ensemble description which will be useful for the analysis of conformational transitions in Tau and other intrinsically disordered proteins.

INTRODUCTION

Tau is a neuronal protein that is critically involved in the pathogenesis of Alzheimer disease and other neurodegenerative diseases termed tauopathies (Avila et al., 2004). A feature shared by tauopathies is that abnormally phosphorylated (hyperphosphorylated) Tau aggregates in the cell, resulting in the accumulation of so-called paired helical filaments. Tau exists in six major splice isoforms in neurons of the CNS (Goedert et al., 1989). The longest Tau isoform with 441 residues contains two N-terminal inserts, a proline-rich region in the center and four C-terminal imperfect repeat domains (termed 2N4R). The best-described function of Tau is the polymerization and stabilization of microtubules (MTs) (Lee and Leugers, 2012; Weingarten et al., 1975). The amino acid sequences in Tau, which interact with MTs, localize to the proline-rich region and the repeat domains, with ^{225}KVAVVR^{230} in the second proline-rich region and the two hexapeptide motifs in repeats R2 and R3 showing the strongest interaction (Kadavath et al., 2015a, 2015b; Mukrasch et al., 2009). Critical for MT binding and polymerization are basic residues such as K225, R230, K274, and K281 (Goode et al., 1997; Goode and Feinstein, 1994).

Phosphorylation and other posttranslational modifications regulate the ability of Tau to bind and assemble MTs (Cohen et al., 2011). Phosphorylation of Tau generally decreases its affinity for MTs and abolishes its ability to stimulate MT polymerization (Cho and Johnson, 2004; Liu et al., 2007), but the specific effects depend on the number and location of phosphorylation sites (Kiris et al., 2011; Liu et al., 2007). Tau contains 85 potential phosphorylation sites, with the three sites S214, T231, and S262 critically important for the Tau-MT interaction. While phosphorylation of S262 strongly reduces the affinity for MTs (Biernat et al., 1993), phosphorylation of S214 (Illenberger et al., 1998) and T231 (Amniai et al., 2009; Cho and Johnson, 2004) primarily decrease the ability of Tau to polymerize MTs (Sillen et al., 2007). Phosphorylation at T231 not only regulates MT binding (Sengupta et al., 1998) but is also important for the role of Tau in disease (Alonso et al., 2010), because it detaches Tau from MTs and thus might enable the interaction with other cellular partners (Frost et al., 2015). Phosphorylation of T231 may also regulate the binding of SH3 domain-containing signaling proteins to the seventh P*XX*P motif (residues P233–P236) of Tau (Reynolds et al., 2008). Several kinases can phosphorylate Tau at T231, including glycogen synthase kinase 3β (GSK3β), which is one of the most important kinases related to the disease process (Lin et al., 2007). GSK3β phosphorylates T231 more efficiently after a priming phosphorylation of S235 (Li et al., 2006), even though this priming phosphorylation is not essential (Lin et al., 2007). Tau deposits isolated from Alzheimer disease patients often contain phosphorylated T231 and S235, as well as phosphorylated S237 and S238 (Hanger and Noble, 2011).

Tau belongs to the class of intrinsically disordered proteins (IDPs) and exists as an ensemble of interconverting structures

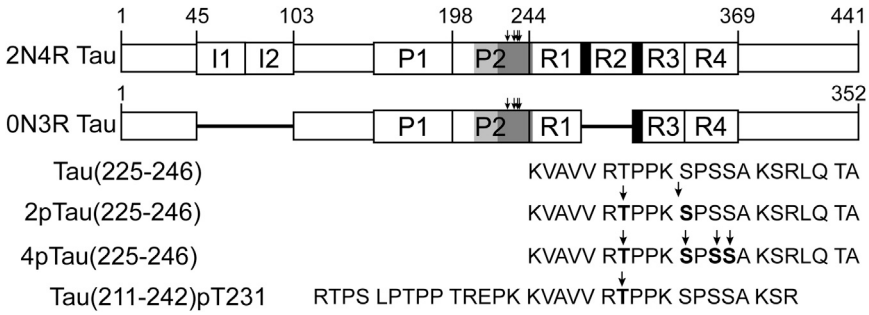

Figure 1. Domain Organization of the Microtubule-Associated Protein Tau

The longest isoform (441 residues, termed 2N4R) contains two N-terminal inserts N1 and N2, the proline-rich regions P1 and P2, and the imperfect repeats R1–R4. In the shortest Tau isoform, 0N3R Tau (352 residues), alternative splicing results in the exclusion of N1, N2, and R2. Below the domain organization, the amino acid sequences of Tau(225–246), T231/S235-phosphorylated Tau(225–246), T231/S235/S237/S238-phosphorylated Tau(225–246), and T231-phosphorylated Tau(211–242) are listed. Dark and light gray shading mark the position of Tau(225–246) and Tau(211–242) within full-length Tau, respectively. Arrows highlight the sites of phosphorylation.

(Mukrasch et al., 2009; Weingarten et al., 1975). In solution, it transiently forms short α-helical, extended, and polyproline II-like elements at specific positions within the sequence (Mukrasch et al., 2009; Schwalbe et al., 2014). Stretches critical for MT binding, such as residues 225–230 in the P2 domain and the aggregation-prone hexapeptides in repeats R2 and R3, exhibit an enhanced propensity to adopt polyproline II-like conformations (Schwalbe et al., 2014). The structural propensities in the repeat domain result in a more extended conformation of this domain than would be expected from a statistical coil model (Mylonas et al., 2008; Schwalbe et al., 2014). Furthermore, Tau samples transient tertiary contacts, the so-called paperclip conformation (Jeganathan et al., 2006). This conformation arises mainly due to long-range, electrostatic interactions between the N terminus and the P2 domain and between the repeat domain and the C terminus, respectively (Mukrasch et al., 2009; Schwalbe et al., 2014).

To obtain an atomic-level description of the structural changes induced by phosphorylation of T231, we studied different Tau fragments as well as full-length Tau by nuclear magnetic resonance (NMR) spectroscopy. We collected an extensive set of structural information on Tau(225–246) in its non-phosphorylated, doubly phosphorylated (T231/S235), and tetra-phosphorylated (T231/S235/S237/S238) state. We then used a novel approach to calculate molecular ensembles based on the NMR data. The molecular ensembles show that phosphorylation of T231 does not perturb the conformation of the critical ^{225}KVAVVR^{230} motif. However, phosphorylation changes the conformation of the basic side chains through formation of a network of salt bridges. The integration of distance and orientational restraints with molecular ensemble calculations, as described here, will be widely applicable to the study of conformational transitions in IDPs.

RESULTS

Phosphorylation at T231/S235 Modulates the Interaction of Tau with MTs

To obtain insight into the effect of phosphorylation at T231/S235 on binding of Tau to MTs, we incubated the Tau isoform 0N3R Tau (also known as fetal Tau or htau23; Figure 1) with MTs at a Tau/tubulin heterodimer ratio of 2:1. Because the interaction of Tau with MTs is intermediate on the NMR timescale (Mukrasch et al., 2009), addition of MTs resulted in changes in NMR signal intensity and position (Figure 2A, black bars). Consistent with observations for 441-residue 2N4R Tau (Kadavath et al., 2015a; Mukrasch et al., 2009), parts of P1, P2, R1, R3, and the C-terminal domain were most attenuated, indicating that these regions facilitate binding to MTs. To analyze the effect of phosphorylation, we used a pseudophosphorylated 0N3R Tau construct, because of the difficulty in preparing homogeneously and site-specifically phosphorylated samples. This construct had residues T231 and S235 mutated to glutamate, and was therefore termed Tau0N3R_E231/E235. Tau0N3R_E231/E235 displayed a MT-binding profile similar to that of the wild-type protein (Figure 2A, gray line). However, resonance intensities in the P2 domain, which contains T231E and S235E, were less attenuated in the presence of MTs, indicating that the MT-interaction mode of these regions is changed. In addition, residues in the neighboring P1 domain and repeat R1 had higher intensities. Notably, pseudophosphorylation had very little effect on the other Tau regions, which are involved in binding to MTs, demonstrating that their binding mode is not altered by pseudophosphorylation at T231/S235.

Next, we performed saturation transfer difference (STD) NMR measurements for Tau(225–246), which contains T231 and S235 and might therefore allow insight into the modified MT interaction of P2. STD NMR showed an efficient transfer of magnetization from MTs to Tau(225–246) (Figure 2B). STD intensities were also detected for Tau(225–246) phosphorylated at either T231/S235 or T231/S235/S237/S238 (Figures 2C and 2D). However, comparison of the STD spectra revealed specific differences between the phosphorylated and non-phosphorylated peptides. The STD spectrum of non-phosphorylated Tau(225–246) was very similar to the regular one-dimensional ^{1}H spectrum (Figure 2B), suggesting tight binding of the whole peptide. In contrast, STD spectra of T231/S235-phosphorylated Tau(225–246) and T231/S235/S237/S238-phosphorylated Tau(225–246) differed from the reference spectrum, with K225-V229 receiving more magnetization than the C-terminal residues (Figures 2C, 2D, and S1A). For example, resonances of the side chain of Q244 and the C-terminal amide protection group (between 6.5 and 7.5 ppm) were more enhanced in Tau(225–246) than in the phosphorylated peptides (Figure S1A). Notably, high-field irradiation did not directly excite Tau resonances as observed in control STD experiments of Tau(225–246) and T231/S235-phosphorylated Tau(225–246) in the absence of microtubules (Figure S1B). Taken together, these data suggest

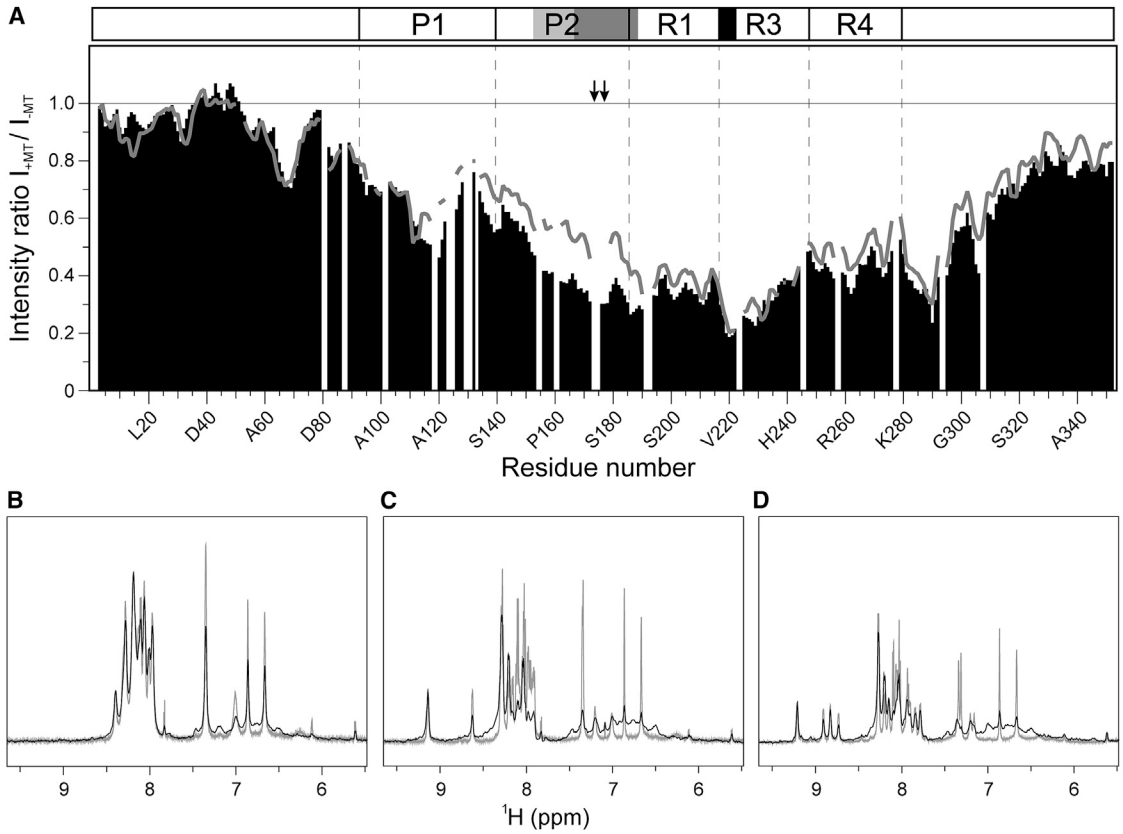

Figure 2. Phosphorylation in the Proline-Rich Region of Tau Modulates Its Interaction with MTs

(A) Residue-specific MT-binding profiles of 0N3R Tau (352 residues; black bars) and pseudophosphorylated 0N3R Tau_E231/E235 (gray line). Intensity ratios were obtained from samples with 20 μM 0N3R Tau in the presence or absence of 10 μM MTs. Small-intensity ratios indicate an interaction of the corresponding residues with MTs. Residue numbering corresponds to that of 0N3R Tau. Pseudophosphorylation of T231 and S235 (marked by black arrows) caused a selective intensity increase in P1 and P2, suggesting a perturbed MT interaction.

(B–D) STD NMR spectra of Tau(225–246) (B), T231/S235-phosphorylated Tau(225–246) (C), and T231/S235/S237/S238-phosphorylated Tau(225–246) (D) in the presence of MTs (molar ratio of 40:1). STD spectra (black contours) were overlaid with reference ^{1}H spectra (gray contours), which were scaled to equal intensities for better comparison. Depending on the phosphorylation state, different amounts of magnetization were transferred, demonstrating that the MT interaction of the proline-rich region of Tau is perturbed upon phosphorylation.

See also Figure S1.

that phosphorylation at T231/S235 and T231/S235/S237/S238 does not inhibit the binding of Tau to MTs, but locally perturbs the MT interaction of Tau residues 230–246.

Phosphorylation Changes the Conformation of the Tau Proline-Rich Region

The aforementioned data show that phosphorylation at T231/S235 locally modulates the binding mode of the P2 domain with MTs. To obtain insight into the molecular basis of these changes, we characterized the structure of Tau(225–246) in its free form. In agreement with previous studies (Palmer and Basak, 2009), circular dichroism showed that irrespective of the number of phosphorylation sites, Tau(225–246) remained mostly disordered in solution (Figure S1C). However, the global minimum was red-shifted upon phosphorylation, in particular in the case of T231/S235/S237/S238-phosphorylated Tau(225–246), indicating a phosphorylation-induced structural change and suggesting that phosphorylation of four residues had a greater effect than phosphorylation of two residues.

To analyze the structure of Tau(225–246) on the single-residue level, we recorded two-dimensional ^{1}H,^{1}H-TOCSY (total correlation spectroscopy), ^{1}H,^{1}H-NOESY (nuclear Overhauser effect spectroscopy), and natural abundance HSQC (heteronuclear single-quantum coherence) spectra. On the basis of these spectra, a nearly complete sequence-specific assignment of the NMR resonances was achieved. Comparison of ^{15}N and C^{α} secondary chemical shifts of Tau(225–246) with values from full-length 2N4R Tau showed a very good agreement between the two constructs (Figures 3A and 3B). Likewise, C^{α} secondary chemical shifts of the T231/S235-phosphorylated Tau(225–246) were very similar to the shifts observed for T231/S235-phosphorylated Tau(208–324) (Sibille et al., 2012) (Figure 3C). The data demonstrate that the conformation adopted by Tau(225–246) (and its phosphorylated variants) is highly similar to the conformation of the same sequence within the full-length protein.

Chemical shifts constitute a rich source of information about the secondary structure and local backbone dynamics of a

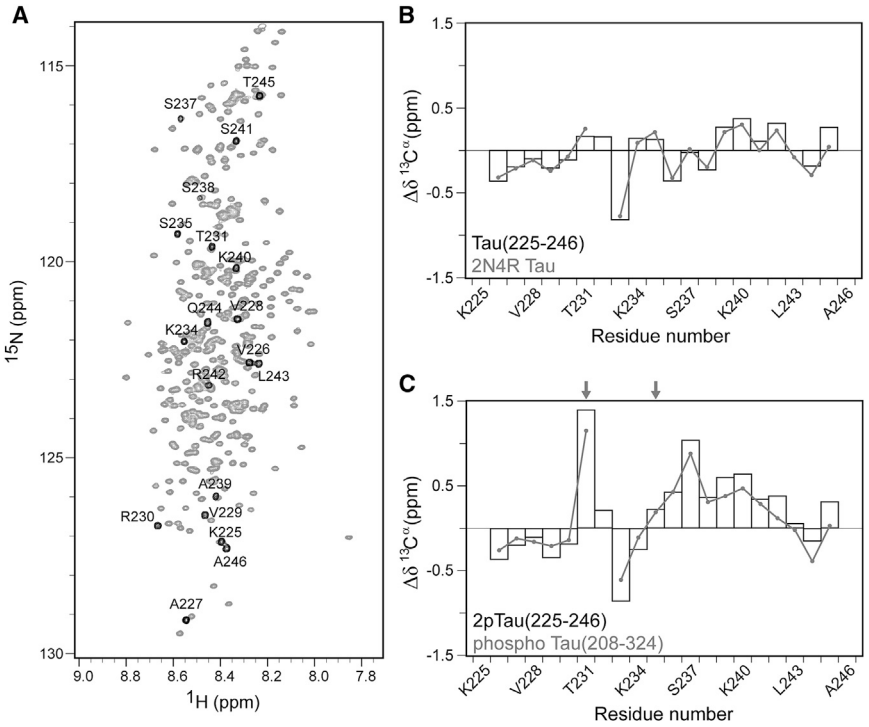

Figure 3. Comparison of the Chemical Environment in Full-Length Tau and Different Tau Constructs

(A) Superposition of two-dimensional ^{1}H,^{15}N-HSQC spectra of 2N4R Tau (441 residues; gray) and Tau(225–246) (black). Selected resonances are labeled.

(B) Residue-specific differences ($\Delta\delta^{13}C^{\alpha}$) between experimental C^{α} chemical shifts and random coil values in 2N4R Tau (gray line) and Tau(225–246) (open bars). The terminal residues K225 and A246 were excluded.

(C) Residue-specific differences between experimental C^{α} chemical shifts and random coil values in T231/S235-phosphorylated Tau(225–246) (open bars) and phosphorylated Tau(208–324) (gray line) (Sibille et al., 2012). Sites of phosphorylation are marked by arrows. Similar $\Delta\delta^{13}C^{\alpha}$ values show that residues in Tau(225–246) adopt the same conformation as within the context of the larger Tau constructs.

protein. Analysis of C^{α}, C^{β}, and H^{α} chemical shifts showed that phosphorylation increased the α-helical propensity of residues A239–R242, which are downstream of the phosphorylation sites (Figure 4A). Combined phosphorylation of T231 and S235 increased the α-helical fraction from about 5% to 15%, while additional phosphorylation of S237 and S238 further raised the α-helical content to ~40%. Consistent with a phosphorylation-induced structuring, chemical shift-derived order parameters revealed a more rigid backbone of S238–R242 upon phosphorylation (Figure 4B). In contrast, structural propensities for residues N-terminal to K234 including the ^{225}KVAVVR^{230} motif remained mostly unaffected by phosphorylation (Figures 4A and 4B).

Residual dipolar couplings (RDCs) provide access to orientational information for individual residues (Bax and Grishaev, 2005; Tjandra and Bax, 1997). Consistent with the observed chemical shifts, RDCs of the backbone amide N-H and C^{α}-H^{α} groups remained largely unchanged for K225–V229 (Figures 4C and 4D). However, $^{1}D_{NH}$ RDCs of V229 and T231 became less negative and the large positive $^{1}D_{C\alpha H\alpha}$ of R230 decreased, indicative of local changes at the C-terminal side of ^{225}KVAVVR^{230} (Figures 4C and 4D). Moreover, residues A239–L243 had fewer negative $^{1}D_{NH}$ RDCs upon phosphorylation at T231 and S235, and even a sign inversion for the same residues in T231/S235/S237/S238-phosphorylated Tau(225–246) (Figure 4C), supporting an enhanced α-helical propensity in the phosphorylated state. Consistent with this finding, a conformational analysis based on both chemical shifts and RDCs using the Flexible-Meccano/ASTEROIDS approach (Ozenne et al., 2012a, 2012b; Salmon et al., 2010), identified an approximately 20% higher propensity for residues S238–R242 to populate α-helical conformations (Figure S2).

The key source for distance information in NMR spectroscopy is the nuclear Overhauser effect (NOE) (Wüthrich, 1986). Analysis of NOESY spectra of Tau(225–246) revealed predominantly short-range sequential NOEs, consistent with a highly dynamic conformation (Figures 5A and 5D). Phosphorylation at T231 and S235, however, almost tripled the number of medium-range NOEs to 35, with the majority of these NOEs arising for residues near the two phosphorylation sites (Figure 5B). This suggests that phosphorylation-induced local structuring in the vicinity of T231 and S235. Introduction of two additional phosphate groups at S237 and S238 drastically increased the number of medium-range NOEs to 117 (Figure 5C). The consecutive pattern of $H^{N}_{i} - H^{N}_{i+2}$, $H^{\alpha}_{i} - H^{N}_{i+2}$, and $H^{\alpha}_{i} - H^{N}_{i+3}$ NOEs supported a phosphorylation-induced α-helical conformation of residues S238–L243. In addition, $H^{\alpha}_{i} - H^{N}_{i+4}$ NOE between S238 and R242 indicated that these residues form the most stable part of the helix.

Determination of Molecular Ensembles

We then used all experimental information consisting of NOESY-derived distance constraints, RDCs, and chemical shifts as restraints for molecular ensemble calculations. We first conducted a series of calculations to optimize the ensemble size, because NOE-based distance restraints are prone to overfitting when the ensemble exceeds two members (Richter et al., 2007). To this end, we used the data set of T231/S235/S237/S238-phosphorylated Tau(225–246), which provided the largest number of NOE restraints, and calculated 100 structures under identical conditions, but increasing the number of ensemble members n from one to ten. The calculations showed that ensembles with $n \geq 2$ perform significantly better than a single structure, which is unable to fulfill all experimental restraints (Figure 5E). A closer inspection of the NOE potential also showed that increasing the ensemble size beyond n = 3 provided no further improvement (Figure 5F, open bars). Similarly, the Q factor, which describes the agreement between experimental and calculated RDCs,

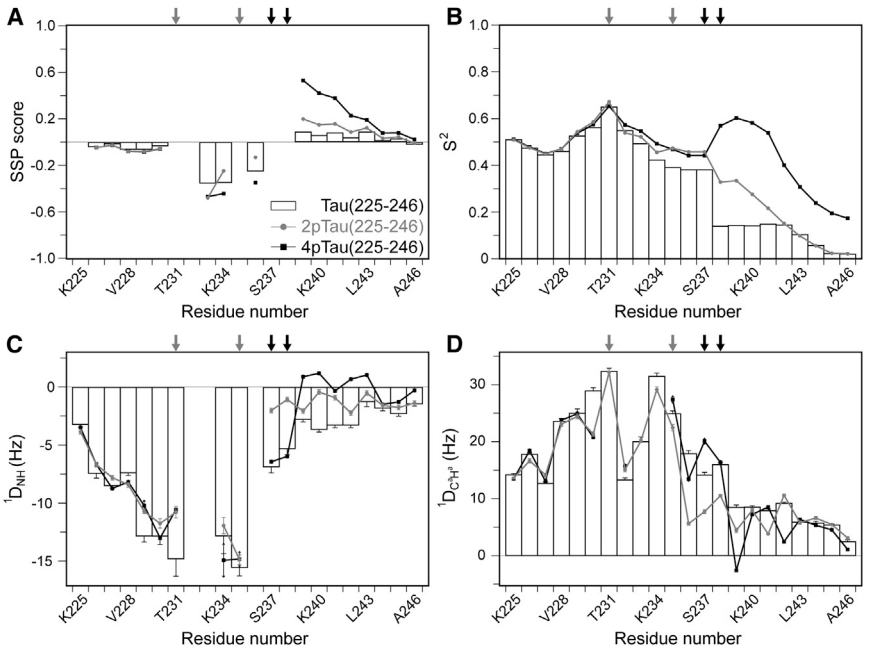

Figure 4. Influence of Phosphorylation on Chemical Shifts and RDCs

(A and B) Secondary structural propensity (SSP) (Marsh et al., 2006) and TALOS-N (Shen and Bax, 2013) analysis of C^{α}, C^{β}, and H^{α} chemical shifts of Tau(225–246) (open bars), T231/S235-phosphorylated Tau(225–246) (gray circles), and T231/S235/S237/S238-phosphorylated Tau(225–246) (black squares). SSP scores represent the fraction of helical (positive values) and extended structure (negative values) at a given residue. (B) Phosphorylation increases the rigidity of residues C-terminal to S237 according to S^2 order parameters derived from TALOS-N.

(C and D) $^{1}D_{NH}$ (C) and $^{1}D_{C\alpha H\alpha}$ (D) RDCs of Tau(225–246) and its two phosphorylated variants. Gaps in (D) arise for residues in T231/S235/S237/S238-phosphorylated Tau(225–246) for which RDCs could not be accurately determined. The same color coding is used in all panels.

Gray arrows indicate the position of the phosphorylated residues T231 and S235, while black arrows mark the position of phosphorylated S237 and S238 in T231/S235/S237/S238-phosphorylated Tau(225–246).

See also Tables S1–S4 and Figure S2. The experimental errors were estimated on the basis of the signal-to-noise ratio in the NMR spectra.

leveled off beyond ensemble sizes of n = 4 (Figure 5F, gray line). We therefore decided to perform all subsequent ensemble calculations with three ensemble members, to benefit from a better agreement with experimental RDCs and at the same time avoid overfitting of the distance restraints.

The resulting ensembles of non-phosphorylated Tau(225–246), T231/S235-phosphorylated Tau(225–246), and T231/S235/S237/S238-phosphorylated Tau(225–246) had similar energies (Figures 5D and 6G–6I). Maximum RDC violations were less than 0.2 Hz for the ensembles, and distance restraint violations did not exceed 0.2 Å. To cross-validate the ensembles, we back-calculated $^{1}J_{H\alpha C\alpha}$ couplings, which had not been used for the ensemble determination. Overall, back-calculated values agreed well with experimentally determined $^{1}J_{H\alpha C\alpha}$ couplings (Figures S3A–S3C), taking into account the accuracy of the corresponding Karplus curve and the random coil $^{1}J_{H\alpha C\alpha}$ values (Vuister et al., 1993; Xiang et al., 2013). In particular, the tendency for larger $^{1}J_{H\alpha C\alpha}$ scalar couplings, which is expected for a helical conformation, was evident for the C-terminal residues in T231/S235/S237/S238-phosphorylated Tau(225–246) (Figure S3D).

Analysis of the 200 lowest-energy structures of Tau(225–246) (Figure 6) in the form of a C^{α} distance probability map (Figure 6A) indicated low probabilities for C^{α} contacts to residues more than two peptide bonds away, in agreement with its dynamic nature. In addition, hydrogen bond probabilities derived from DSSP (Kabsch and Sander, 1983) showed that the non-phosphorylated main chain has a negligible tendency to form CO_i-$HN_{i\,+\,3/4/5}$ hydrogen bonds (Figure 6D). Representative ensembles of Tau(225–246) are shown in Figure 6G. Notably, we observed a ~30% probability for a C^{α} contact between P236 and A239 (Figure 6A), which may reflect the intrinsic propensity of this region to form a helical conformation.

Despite the newly observed medium-range NOEs (Figure 5B) and RDC changes (Figures 4C and 4D), the C^{α} distance probability map of T231/S235-phosphorylated Tau(225–246) showed only modest differences when compared with the non-phosphorylated state (Figure 6B). The enhanced probabilities for $C^{\alpha}_{i} - C^{\alpha}_{i+3}$ contacts (increased by ~10%–15%) and hydrogen bonds (increased by ~5%) (Figures 6B and 6E) for K240–Q244 reflect an increased helical propensity of these residues. At the same time, phosphorylation of T231 and S235 abolished the ~30% probability for the C^{α} contact between P236 and A239 (Figure 6B). Introduction of additional phosphate groups at S237 and S238 strongly enhanced the probabilities for $C^{\alpha}_{i} - C^{\alpha}_{i+3}$ and $C^{\alpha}_{i} - C^{\alpha}_{i+4}$ contacts (Figure 6C), as well as CO_i-$HN_{i\,+\,3/4/5}$ hydrogen bonds for A239–Q244 (Figure 6F). The results clearly support the helical character of this region (Figure 6I), but cannot distinguish between an α or 3_{10} helix. In addition, the ~60% probability for $C^{\alpha}_{i} - C^{\alpha}_{i+4}$ contacts suggests that the helix forms transiently. For the ^{225}KVAVVR^{230} MT-binding motif, which is located N-terminal to the phosphorylated T231, the C^{α} distance probability maps of T231/S235-phosphorylated Tau(225–246) and T231/S235/S237/S238-phosphorylated Tau(225–246) showed little difference (Figures 6G–6I), although slightly increased probabilities for $C^{\alpha}_{i} - C^{\alpha}_{i+2}$ contacts (Figures 6A and 6B) suggest a compaction of V229–P232 upon phosphorylation.

Salt Bridge Formation due to Phosphorylation of T231

While phosphorylation of T231 had little effect on the backbone conformation of the ^{225}KVAVVR^{230} MT-binding region (Figure 6), we found that arginine and lysine side chain resonances were perturbed (Figure 7). Non-phosphorylated Tau(225–246) lacks acidic residues. It is therefore unable to form salt bridges, and has narrow chemical shift dispersion and low intensities of the

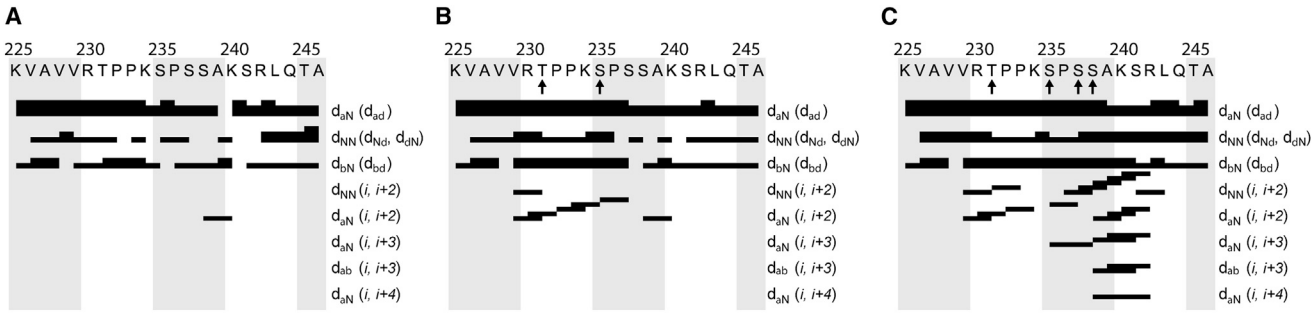

D

	Tau(225-246)	2pTau(225-246)	4pTau(225-246)
Experimental restraints			
short-range NOEs	123	123	154
medium-range NOEs	13	35	117
RDC $^{1}D_{NH}/^{1}D_{C^{a}H^{a}}$	19/22	19/22	19/19
C^{a}/C^{b} chemical shifts	20/20	14/14	11/11
Statistics of Ensemble calculation			
Total target energy	81.18	91.13	83.59
CARB Potential energy	5.80	3.71	2.36
NOE Potential energy	0.42	0.98	1.74
SARDC Potential energy	0.41	0.61	0.34
Q-factor	0.267	0.178	0.177

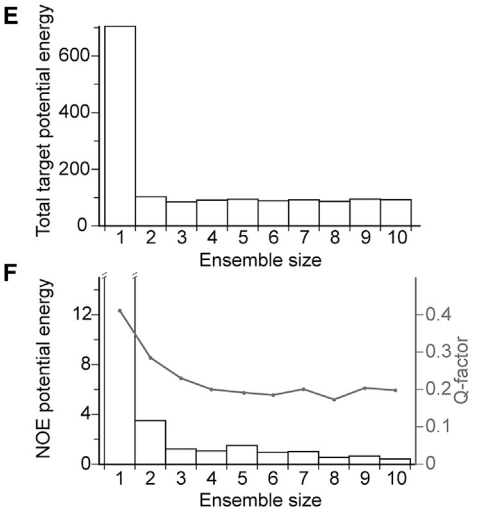

Figure 5. Phosphorylation-Induced Restructuring Results in a Large Number of Interproton Contacts

(A–C) Medium and short-range NOE contacts observed in Tau(225–246) in its non-phosphorylated (A), T231/S235-phosphorylated (B), and T231/S235/S237/S238-phosphorylated (C) states. For short-range NOEs (first three rows), the height of the black bars classifies the respective NOE as strong, medium, or weak. Black arrows below the amino acid sequence mark the sites of phosphorylation. Protons, which gave rise to the NOE contacts, are indicated to the right.

(D) Overview of experimental restraints and structural statistics in Tau(225–246) as a function of the phosphorylation state. Q factor represents the quality factor between experimental RDCs and values back-calculated from the molecular ensembles.

(E) Influence of the ensemble size on the overall energy of the conformations. A single structure was not able to fulfill all experimental restraints.

(F) Good agreement between experimental NOE distance restraints and distances observed in the calculated conformations (open bars), as well as between experimental and back-calculated RDCs (gray line), was observed for ensemble sizes of $n \geq 3$.

See also Figure S3.

distal side-chain nuclei (e.g., H^{ε}) of its basic residues (Figure 7A). In contrast, phosphorylation of T231 and S235 resulted in chemical shift changes of the side chains of R230 and K234, suggesting that these two residues interacted with a phosphate group. R230 especially displayed a strongly downfield shift and sharpened H^{ε}-N^{ε} cross peak (Figure 7A). The assignment of the H^{ε} atoms to particular arginine residues is shown in Figures S4 and S5. To elucidate which phosphate group interacts with which basic group, we used the peptide Tau(211–242) phosphorylated only at T231. This Tau fragment displayed the same specific shift for R230 as T231/S235-phosphorylated Tau(225–242) (Figure 7B), suggesting that T231 specifically forms a salt bridge with the preceding R230. Notably, none of the other basic residues in T231-phosphorylated Tau(211–242) (three arginines and four lysines) showed any indication for salt bridge formation. Analysis of the secondary C^{α} chemical shifts of Tau(211–242) exclusively phosphorylated at T231 further showed that it has minimal α-helical propensity at its C terminus, similar to non-phosphorylated Tau(225–246) (Figure 7C). This indicates that the increase in α-helical propensity of T231/S235-phosphorylated Tau(225–246) and T231/S235/S237/S238-phosphorylated Tau(225–246) is independent of phosphorylation of T231, but rather depends on the phosphorylation of S235, S237, and S238.

In the case of tetra-phosphorylated Tau(225–246), additional chemical shift changes were observed for K240 and R242 (Figures 7A and S6), suggesting that the latter two basic residues form salt bridges with the phosphate groups of S237 and S238. The signal enhancement in the NOESY spectrum of T231/S235/S237/S238-phosphorylated Tau(225–246) relative to T231/S235-phosphorylated Tau(225–246) further indicated that the salt bridges were more stable upon phosphorylation of S237 and S238 (Figures S4 and S6).

We next analyzed our calculated ensembles with respect to the formation of salt bridges. Note that the ensemble calculations did not consider electrostatics or include distance restraints between basic and acidic groups to specify salt bridges.

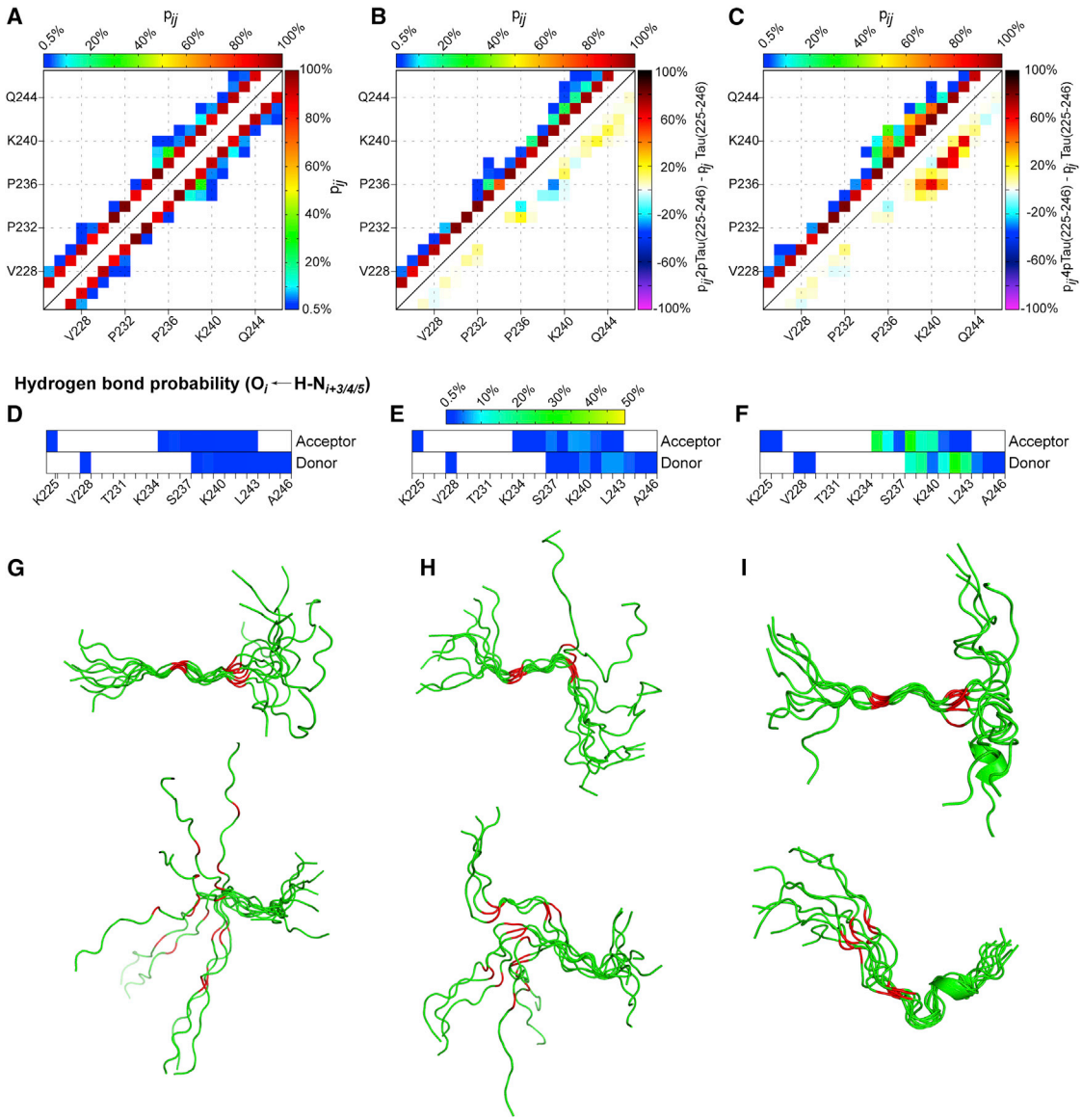

Figure 6. Molecular Ensembles of Non-phosphorylated and Phosphorylated Tau(225–246)

(A–C) C^{α} distance probability maps for the 200 lowest-energy structures of the molecular ensembles (600 individual conformers) of non-phosphorylated (A), T231/S235-phosphorylated (B), and T231/S235/S237/S238-phosphorylated (C) Tau(225–246). $C^{\alpha}{}_{i} - C^{\alpha}{}_{i+1}$ distances were generally below 7 Å and were omitted from the diagram. To highlight differences with respect to non-phosphorylated Tau(225–246), difference maps are given below the diagonal in the case of phosphorylated variants.

(D–F) Probability of each residue to be a hydrogen bond acceptor or donor in the molecular ensembles of non-phosphorylated (D), T231/S235-phosphorylated (E), and T231/S235/S237/S238-phosphorylated (F) Tau(225–246). Only hydrogen bonds between the main chain carbonyl oxygen of residue *i* and the main chain amide group of residues *i* + 3, *i* + 4, and *i* + 5 were considered. Hydrogen bonds in the 200 lowest-energy structures were derived using DSSP (Kabsch and Sander, 1983).

(G–I) Backbone conformation of the three lowest-energy structures of non-phosphorylated (G), T231/S235-phosphorylated (H), and T231/S235/S237/S238-phosphorylated (I) Tau(225–246). In the top row, structures were aligned to residues V229–K234, while S237–R242 was superimposed in the lower row. Structures are shown with the N terminus to the left. T231 and S235 are highlighted in red.

See also Figures S4 and S5.

To determine the occurrence of salt bridges, we defined the maximum distance between the phosphate atom and the nitrogen atom in the basic groups of arginine and lysine to 4.5 Å. In agreement with the observation in the NMR spectra, the phosphate groups of T231 and S235 in the T231/S235-phosphorylated Tau(225–246) ensemble primarily formed salt bridges with the directly preceding basic residues R230 and K234, respectively (Figure 7D). For the T231/S235/S237/S238-phosphorylated Tau(225–246) ensemble, the phosphate group of T231 predominantly formed a salt bridge with R230, while the

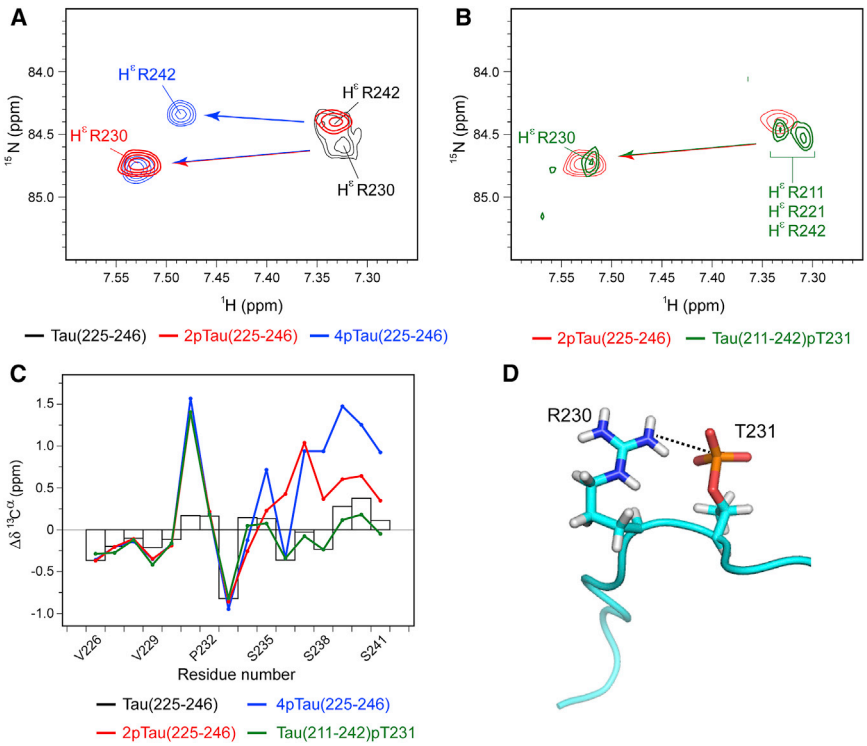

Figure 7. Electrostatic Interactions in the Proline-Rich Domain of Tau due to Phosphorylation at T231

(A) ^{1}H,^{15}N-HSQC spectrum showing the spectral region of the guanidinium group of arginine side chains. Due to missing interactions with negatively charged groups in the non-phosphorylated state, the signals for the $H^{\varepsilon}N^{\varepsilon}$ groups of R230 and R242 have weak intensities and display low signal dispersion (black). Phosphorylation of T231 and S235 resulted in a selective downfield shift of R230 (red), while R242 remained unaffected. Additional phosphorylation of S237 and S238 caused an almost identical shift for R230, but also moved the resonance of R242 (blue). The resonance shifts were accompanied by enhanced peak intensities.

(B) Comparison of the ^{1}H,^{15}N-HSQC spectrum of Tau(211–242) phosphorylated at T231 (green) with that of Tau(225–246) phosphorylated at T231 and S235 (red) showed that single phosphorylation of T231 results in the same selective shift of R230. Resonances of the other three arginine residues remained unaffected.

(C) Single phosphorylation of T231 does not stabilize helical structure in the proline-rich region of Tau according to C^{α} secondary chemical shifts in T231-phosphorylated Tau(211–242) (green line). For comparison, C^{α} secondary chemical shifts in other phosphorylation states are shown.

(D) Representative conformation selected from the molecular ensemble, which was calculated for Tau(225–246) phosphorylated at T231 and S235. The side chain of R230 and the phosphate group at position 231 (red) are highlighted. The black dashed line marks the potential position of the salt bridge between R230 and T231.

See also Figure S6.

two additional phosphate groups at S237 and S238 preferentially formed salt bridges with distant residues K234 and R242, respectively. The medium-range nature of these salt bridges may be responsible for the stabilization of the α-helical conformation in the proline-rich region of Tau, because the side chains of S238 and R242 would locate to the same sides of the helix, thus favoring salt bridge formation.

DISCUSSION

The high degree of disorder in Tau and other IDPs complicates the analysis of conformational transitions, which occur in these proteins during physiological and pathological processes. NMR spectroscopy is the most powerful tool for the characterization of these processes, as it provides a wealth of information about both the secondary and tertiary structure with single-residue resolution (Dyson and Wright, 2004). At the same time, the rapid exchange between multiple conformations requires interpretation of the NMR observables in terms of ensembles (Fisher and Stultz, 2011; Jensen et al., 2014; Mittag et al., 2010). To this end, molecular dynamics simulations and sample-and-select approaches were developed, whereby sub-ensembles are derived from a broader distribution (Allison et al., 2009; Fisher and Stultz, 2011; Jensen et al., 2014; Mittag et al., 2010; Xiang et al., 2013). However, these approaches focused on the use of chemical shifts and RDCs as experimental restraints. Here, we took the next step and included a large number of distance restraints derived from experimental NOE contacts. Inclusion of NOE distance information in the calculation of molecular ensembles of IDP is not only important as the NOE effect represents the most important structural restraint in NMR-based structural biology (Wüthrich, 1986), but also because ensemble descriptions of IDPs are highly underdetermined due to the inherently large number of degrees of conformational freedom (Allison et al., 2009; Fisher and Stultz, 2011; Jensen et al., 2014; Mittag and Forman-Kay, 2007; Xiang et al., 2013). Thus, while long-range NOEs are difficult to observe in IDPs, the presence and modulation of local structure can be accurately described by medium-range NOE contacts. Long-range distance information from paramagnetic spin labels (Gillespie and Shortle, 1997) can be included just as distance information from NOEs into the ensemble calculation protocol. In addition, potentials for refinement against small-angle X-ray scattering data are available (Schwieters and Clore, 2014), allowing to further restrict the sampled volume space (Sibille and Bernado, 2012).

Phosphorylation of the proline-rich domain of Tau, especially at T231, regulates assembly of tubulin into microtubules (Cho and Johnson, 2004; Sengupta et al., 1998). The aim of this study was therefore to determine the structural changes induced in Tau upon phosphorylation of T231 and three neighboring sites. To this end, we combined NMR-derived distance information, RDCs, and chemical shifts to calculate ensembles of conformations in different phosphorylation states. In agreement with previous reports (Amniai et al., 2009; Cho and Johnson, 2004), we

found that introduction of up to four phosphate groups did not abolish binding of the proline-rich region of Tau to MTs, but changed the mode of interaction. We also found that phosphorylation had only a limited effect on the backbone conformation of the MT-binding motif ^{225}KVAVVR^{230}. Instead, phosphorylation of T231 resulted in the formation of a salt bridge between the phosphate group of T231 and the basic side chain of R230. Because R230 is important for MT binding and assembly (Goode et al., 1997), we propose that the intramolecular salt bridge between T231 and R230 competes with the formation of intermolecular salt bridges to MTs and prevents the ^{225}KVAVVR^{230} motif from adopting a binding-competent conformation.

Double phosphorylation of T231 and S235 was previously proposed to induce a β turn for residues V229–T231 (Daly et al., 2000). In addition, introduction of further phosphate groups was suggested to increase the polyproline II helix population in the proline-rich region P2 (Bielska and Zondlo, 2006). In contrast, NMR chemical shifts and molecular dynamics simulations indicated that in vitro phosphorylation of Tau at T231 and S235 stabilizes an α helix between residues P236 and L243 (Lyons et al., 2014; Sibille et al., 2012). Our molecular ensemble calculations of different phosphorylation states of the proline-rich region P2 support a phosphorylation-induced stabilization of a transient helical structure of residues A239–R242. The transient helical structure, however, is independent of phosphorylation of T231 and only depends on the phosphorylation of S235, S237, and S238. Because MT assembly is modulated by the phosphorylation of T231 (Amniai et al., 2009; Cho and Johnson, 2004), our data indicate that stabilization of the helical conformation is not responsible for the effect of T231 phosphorylation on Tau-mediated MT assembly. On the other hand, it might affect the interaction of the conserved P233-*XX*-P236 motif with SH3 domain-containing proteins (Reynolds et al., 2008). Notably, the ensemble calculations showed neither an enhanced propensity for $C^{\alpha}_{i} - C^{\alpha}_{i+3}$ distances of less than 7 Å nor an increased occurrence of CO_i–NH_{i+3} hydrogen bonds for residues V229–T231, interactions that would support a β-turn formation of residues V229–T231.

Conclusions

Employing an extensive set of distance and orientational restraints together with a novel ensemble calculation approach, we determined molecular ensembles of Tau fragments in the non-phosphorylated state and when phosphorylated at T231/S235 or T231/S235/S237/S238. The molecular ensembles showed that phosphorylated T231, a key site in Alzheimer disease, selectively engages in a salt bridge with R230 that can compete with the formation of intermolecular salt bridges to tubulin. We further showed that a transient helix between S238 and R242 is stabilized by phosphorylation of S235, S237, and S238, but is independent of phosphorylation at T231. Integration of distance and orientational restraints with molecular ensemble calculations, as described here, will be highly useful for the analysis of conformational transitions in IDPs.

EXPERIMENTAL PROCEDURES

Sample Preparation

^{15}N-Labeled 0N3R Tau and its pseudophosphorylated variant, in which residues T231 and S235 (numbering of residues by analogy with the longest CNS isoform, 2N4R) were replaced by glutamate (called 0N3R Tau_E231/E235), were expressed in *Escherichia coli* using M9 minimal medium according to established protocols (Mukrasch et al., 2009).

Tau peptides were produced by standard Fmoc-solid-phase peptide synthesis using an ABI 433A synthesizer (Applied Biosystems). Phosphorylated threonine and serine residues were introduced at positions T231 and S235 for 2pTau(225–246), and at T231, S235, S237, and S238 for 4pTau(225–246). Peptides were synthesized with acetyl and amide protection groups at the N and C termini, respectively, and purified by reversed-phase high-performance liquid chromatography. T231-phosphorylated Tau(211–242) was obtained from EZBiolab.

Ensemble Calculation

Conformational ensembles were calculated using the ensemble calculation protocol implemented in XPLOR-NIH (version 2.34) (Schwieters et al., 2006, 2003). Extended starting structures of non-phosphorylated Tau(225–246), T231/S235-phosphorylated Tau(225–246), and T231/S235/S237/S238-phosphorylated Tau(225–246) were created and parameterized through a standard script available in the XPLOR-NIH distribution. For ensemble calculation, the simulated annealing protocol provided in the *sardc* (Huang and Grzesiek, 2009) tutorial was used and modified to include potentials representing experimental distance (NOE), RDC, and chemical shift (C^{α} and C^{β}) restraints. Chemical shifts of the phosphorylated residues, and of their direct predecessors and successors, were excluded from the calculations due to missing chemical shift corrections for phosphorylated residues in XPLOR-NIH. Distance restraints were derived from NOE cross peaks observed in NOESY spectra with mixing times of 300 ms. Cross-peak intensities were converted into distances using protocols implemented in CYANA (Herrmann et al., 2002). The distance restraints were then divided into two groups. The first group consisted of sequential *i* to *i* + 1 NOEs with distance boundaries of 2.8–4.0 Å, and had to be satisfied by all individual conformers. All other NOEs of the second group were classified into four categories and were subject to ensemble averaging. These NOEs were classified as (1) strong, (2) medium, (3) weak, and (4) very weak, with distance boundaries of 1.8–2.7, 1.8–3.5, 1.8–5.0, and 1.8–6.0 Å, respectively. In addition, standard XPLOR-NIH potentials representing bond length, bond angle, improper dihedral, and non-bonded repulsive terms were used. The XPLOR-NIH potential for torsion angles was not used, as it might bias the ensemble to angles observed for globular proteins.

Starting structures were copied n times according to the ensemble size and individually randomized by torsion angle dynamics for 50 ps at 3,003 K. Simulated annealing started at 3,003 K and was followed by cooling to 278 K in 12.5-K decrements. During annealing, all potentials named above were applied and the scaling factors gradually ramped up. Subsequently, ensembles were energy minimized in torsion angle space and Cartesian space. All torsion angle dynamics used the internal variable module (Schwieters and Clore, 2001). For all Tau(225–246) peptides, 800 structures with three ensemble members were calculated, giving rise to 2,400 individual conformers. To validate the ensemble structures, $^{1}J_{H\alpha C\alpha}$ couplings were back-calculated using the procedure described by Xiang et al. (2013) and compared with experimental values. To this end, the backbone torsion angles ϕ and ψ of each individual conformer were determined using MOLMOL (Koradi et al., 1996). From the obtained angles, $^{1}J_{H\alpha C\alpha}$ couplings were calculated and the resulting couplings averaged over the ensemble. To calculate C^{α} contact probability maps of the 200 lowest-energy structures, the *contactMap* script of XPLOR-NIH was used with the distance cut-off set to 7 Å.

SUPPLEMENTAL INFORMATION

Supplemental Information includes four tables and six figures and can be found with this article online at http://dx.doi.org/10.1016/j.str.2015.06.002.

AUTHOR CONTRIBUTIONS

M.S. performed sample preparation, data acquisition, data analysis, and structure calculations, and wrote the paper. H.K. performed microtubules measurements. J.B. contributed to sample preparation. V.O. and M.B. performed Meccano calculations. E.M. supervised sample production. M.Z. designed and supervised the project and wrote the paper.

ACKNOWLEDGMENTS

M.Z. was supported by Deutsche Forschungsgemeinschaft through project ZW 71/8-1. We thank Christian Griesinger and Eva Mandelkow for discussions, Sabrina Hübschmann for sample preparations, and Kerstin Overkamp for peptide synthesis.

Received: March 23, 2015
Revised: June 5, 2015
Accepted: June 8, 2015
Published: July 9, 2015

REFERENCES

Allison, J.R., Varnai, P., Dobson, C.M., and Vendruscolo, M. (2009). Determination of the free energy landscape of alpha-synuclein using spin label nuclear magnetic resonance measurements. J. Am. Chem. Soc. *131*, 18314–18326.

Alonso, A.D., Di Clerico, J., Li, B., Corbo, C.P., Alaniz, M.E., Grundke-Iqbal, I., and Iqbal, K. (2010). Phosphorylation of Tau at Thr(212), Thr(231), and Ser(262) combined causes neurodegeneration. J. Biol. Chem. *285*, 30851–30860.

Amniai, L., Barbier, P., Sillen, A., Wieruszeski, J.-M., Peyrot, V., Lippens, G., and Landrieu, I. (2009). Alzheimer disease specific phosphoepitopes of Tau interfere with assembly of tubulin but not binding to microtubules. FASEB J. *23*, 1146–1152.

Avila, J., Lucas, J.J., Perez, M., and Hernandez, F. (2004). Role of tau protein in both physiological and pathological conditions. Physiol. Rev. *84*, 361–384.

Bax, A., and Grishaev, A. (2005). Weak alignment NMR: a hawk-eyed view of biomolecular structure. Curr. Opin. Struct. Biol. *15*, 563–570.

Bielska, A.A., and Zondlo, N.J. (2006). Hyperphosphorylation of tau induces local polyproline II helix. Biochemistry *45*, 5527–5537.

Biernat, J., Gustke, N., Drewes, G., Mandelkow, E.M., and Mandelkow, E. (1993). Phosphorylation of Ser262 strongly reduces binding of tau to microtubules: distinction between PHF-like immunoreactivity and microtubule binding. Neuron *11*, 153–163.

Cho, J.-H., and Johnson, G.V.W. (2004). Primed phosphorylation of tau at Thr231 by glycogen synthase kinase 3β (GSK3β) plays a critical role in regulating tau's ability to bind and stabilize microtubules. J. Neurochem. *88*, 349–358.

Cohen, T.J., Guo, J.L., Hurtado, D.E., Kwong, L.K., Mills, I.P., Trojanowski, J.Q., and Lee, V.M.Y. (2011). The acetylation of tau inhibits its function and promotes pathological tau aggregation. Nat. Commun. *2*, 252.

Daly, N.L., Hoffmann, R., Otvos, L., and Craik, D.J. (2000). Role of phosphorylation in the conformation of tau peptides implicated in Alzheimer's disease. Biochemistry *39*, 9039–9046.

Dyson, H.J., and Wright, P.E. (2004). Unfolded proteins and protein folding studied by NMR. Chem. Rev. *104*, 3607–3622.

Fisher, C.K., and Stultz, C.M. (2011). Constructing ensembles for intrinsically disordered proteins. Curr. Opin. Struct. Biol. *21*, 426–431.

Frost, B., Götz, J., and Feany, M.B. (2015). Connecting the dots between tau dysfunction and neurodegeneration. Trends Cell Biol. *25*, 46–53.

Gillespie, J.R., and Shortle, D. (1997). Characterization of long-range structure in the denatured state of staphylococcal nuclease. II. Distance restraints from paramagnetic relaxation and calculation of an ensemble of structures. J. Mol. Biol. *268*, 170–184.

Goedert, M., Spillantini, M.G., Jakes, R., Rutherford, D., and Crowther, R.A. (1989). Multiple isoforms of human microtubule-associated protein tau: sequences and localization in neurofibrillary tangles of Alzheimer's disease. Neuron *3*, 519–526.

Goode, B.L., and Feinstein, S.C. (1994). Identification of a novel microtubule-binding and assembly domain in the developmentally-regulated inter-repeat region of tau. J. Cell Biol. *124*, 769–782.

Goode, B.L., Denis, P.E., Panda, D., Radeke, M.J., Miller, H.P., Wilson, L., and Feinstein, S.C. (1997). Functional interactions between the proline-rich and repeat regions of tau enhance microtubule binding and assembly. Mol. Biol. Cell *8*, 353–365.

Hanger, D.P., and Noble, W. (2011). Functional implications of glycogen synthase kinase-3-mediated tau phosphorylation. Int. J. Alzheimers Dis. *2011*, 352805.

Herrmann, T., Güntert, P., and Wüthrich, K. (2002). Protein NMR structure determination with automated NOE assignment using the new software CANDID and the torsion angle dynamics algorithm DYANA. J. Mol. Biol. *319*, 209–227.

Huang, J.-R., and Grzesiek, S. (2009). Ensemble calculations of unstructured proteins constrained by RDC and PRE data: a case study of urea-denatured ubiquitin. J. Am. Chem. Soc. *132*, 694–705.

Illenberger, S., Zheng-Fischhöfer, Q., Preuss, U., Stamer, K., Baumann, K., Trinczek, B., Biernat, J., Godemann, R., Mandelkow, E.-M., and Mandelkow, E. (1998). The endogenous and cell cycle-dependent phosphorylation of tau protein in living cells: implications for Alzheimer's disease. Mol. Biol. Cell *9*, 1495–1512.

Jeganathan, S., von Bergen, M., Brutlach, H., Steinhoff, H.J., and Mandelkow, E. (2006). Global hairpin folding of tau in solution. Biochemistry *45*, 2283–2293.

Jensen, M.R., Zweckstetter, M., Huang, J.R., and Backledge, M. (2014). Exploring free-energy landscapes of intrinsically disordered proteins at atomic resolution using NMR spectroscopy. Chem. Rev. *114*, 6632–6660.

Kabsch, W., and Sander, C. (1983). Dictionary of protein secondary structure: pattern recognition of hydrogen-bonded and geometrical features. Biopolymers *22*, 2577–2637.

Kadavath, H., Hofele, R.V., Biernat, J., Kumar, S., Tepper, K., Urlaub, H., Mandelkow, E., and Zweckstetter, M. (2015a). Tau stabilizes microtubules by binding at the interface between tubulin heterodimers. Proc. Natl. Acad. Sci. USA *112*, 7501–7506.

Kadavath, H., Jaremko, M., Jaremko, L., Biernat, J., Mandelkow, E., and Zweckstetter, M. (2015b). Folding of tau on microtubules. Angew. Chem. Int. Ed. Engl. (in press). http://dx.doi.org/10.1002/anie.201501714.

Kiris, E., Ventimiglia, D., Sargin, M.E., Gaylord, M.R., Altinok, A., Rose, K., Manjunath, B.S., Jordan, M.A., Wilson, L., and Feinstein, S.C. (2011). Combinatorial Tau pseudophosphorylation: markedly different regulatory effects on microtubule assembly and dynamic instability than the sum of the individual parts. J. Biol. Chem. *286*, 14257–14270.

Koradi, R., Billeter, M., and Wüthrich, K. (1996). MOLMOL: a program for display and analysis of macromolecular structures. J. Mol. Graph. *14*, 51–55.

Lee, G., and Leugers, C.J. (2012). Tau and tauopathies. Prog. Mol. Biol. Transl. Sci. *107*, 263–293.

Li, T., Hawkes, C., Qureshi, H.Y., Kar, S., and Paudel, H.K. (2006). Cyclin-dependent protein kinase 5 primes microtubule-associated protein tau site-specifically for glycogen synthase kinase 3β. Biochemistry *45*, 3134–3145.

Lin, Y.-T., Cheng, J.-T., Liang, L.-C., Ko, C.-Y., Lo, Y.-K., and Lu, P.-J. (2007). The binding and phosphorylation of Thr231 is critical for Tau's hyperphosphorylation and functional regulation by glycogen synthase kinase 3β. J. Neurochem. *103*, 802–813.

Liu, F., Li, B., Tung, E.J., Grundke-Iqbal, I., Iqbal, K., and Gong, C.X. (2007). Site-specific effects of tau phosphorylation on its microtubule assembly activity and self-aggregation. Eur. J. Neurosci. *26*, 3429–3436.

Lyons, A.J., Gandhi, N.S., and Mancera, R.L. (2014). Molecular dynamics simulation of the phosphorylation-induced conformational changes of a tau peptide fragment. Proteins *82*, 1907–1923.

Marsh, J.A., Singh, V.K., Jia, Z., and Forman-Kay, J.D. (2006). Sensitivity of secondary structure propensities to sequence differences between α- and γ-synuclein: implications for fibrillation. Protein Sci. *15*, 2795–2804.

Mittag, T., and Forman-Kay, J.D. (2007). Atomic-level characterization of disordered protein ensembles. Curr. Opin. Struct. Biol. *17*, 3–14.

Mittag, T., Kay, L.E., and Forman-Kay, J.D. (2010). Protein dynamics and conformational disorder in molecular recognition. J. Mol. Recognit. *23*, 105–116.

Mukrasch, M.D., Bibow, S., Korukottu, J., Jeganathan, S., Biernat, J., Griesinger, C., Mandelkow, E., and Zweckstetter, M. (2009). Structural polymorphism of 441-residue tau at single residue resolution. PLoS Biol. *7*, e34.

Mylonas, E., Hascher, A., Bernado, P., Blackledge, M., Mandelkow, E., and Svergun, D.I. (2008). Domain conformation of tau protein studied by solution small-angle X-ray scattering. Biochemistry *47*, 10345–10353.

Ozenne, V., Bauer, F., Salmon, L., Huang, J.R., Jensen, M.R., Segard, S., Bernado, P., Charavay, C., and Blackledge, M. (2012a). Flexible-meccano: a tool for the generation of explicit ensemble descriptions of intrinsically disordered proteins and their associated experimental observables. Bioinformatics *28*, 1463–1470.

Ozenne, V., Schneider, R., Yao, M., Huang, J.R., Salmon, L., Zweckstetter, M., Jensen, M.R., and Blackledge, M. (2012b). Mapping the potential energy landscape of intrinsically disordered proteins at amino acid resolution. J. Am. Chem. Soc. *134*, 15138–15148.

Palmer, H., and Basak, A. (2009). Effect of phosphorylation on tau aggregation using model peptides and circular dichroism studies. Adv. Exp. Med. Biol. *611*, 259–261.

Reynolds, C.H., Garwood, C.J., Wray, S., Price, C., Kellie, S., Perera, T., Zvelebil, M., Yang, A., Sheppard, P.W., Varndell, I.M., et al. (2008). Phosphorylation regulates tau interactions with Src homology 3 domains of phosphatidylinositol 3-kinase, phospholipase Cgamma1, Grb2, and Src family kinases. J. Biol. Chem. *283*, 18177–18186.

Richter, B., Gsponer, J., Várnai, P., Salvatella, X., and Vendruscolo, M. (2007). The MUMO (minimal under-restraining minimal over-restraining) method for the determination of native state ensembles of proteins. J. Biomol. NMR *37*, 117–135.

Salmon, L., Nodet, G., Ozenne, V., Yin, G., Jensen, M.R., Zweckstetter, M., and Blackledge, M. (2010). NMR characterization of long-range order in intrinsically disordered proteins. J. Am. Chem. Soc. *132*, 8407–8418.

Schwalbe, M., Ozenne, V., Bibow, S., Jaremko, M., Jaremko, L., Gajda, M., Jensen, M.R., Biernat, J., Becker, S., Mandelkow, E., et al. (2014). Predictive atomic resolution descriptions of intrinsically disordered hTau40 and alpha-synuclein in solution from NMR and small angle scattering. Structure *22*, 238–249.

Schwieters, C.D., and Clore, G.M. (2001). Internal coordinates for molecular dynamics and minimization in structure determination and refinement. J. Magn. Reson. *152*, 288–302.

Schwieters, C.D., and Clore, G.M. (2014). Using small angle solution scattering data in Xplor-NIH structure calculations. Prog. Nucl. Magn. Reson. Spectrosc. *80*, 1–11.

Schwieters, C.D., Kuszewski, J.J., Tjandra, N., and Marius Clore, G. (2003). The Xplor-NIH NMR molecular structure determination package. J. Magn. Reson. *160*, 65–73.

Schwieters, C.D., Kuszewski, J.J., and Marius Clore, G. (2006). Using Xplor-NIH for NMR molecular structure determination. Prog. Nucl. Magn. Reson. Spectrosc. *48*, 47–62.

Sengupta, A., Kabat, J., Novak, M., Wu, Q.L., Grundke-Iqbal, I., and Iqbal, K. (1998). Phosphorylation of tau at both Thr 231 and Ser 262 is required for maximal inhibition of its binding to microtubules. Arch. Biochem. Biophys. *357*, 299–309.

Shen, Y., and Bax, A. (2013). Protein backbone and sidechain torsion angles predicted from NMR chemical shifts using artificial neural networks. J. Biomol. NMR *56*, 227–241.

Sibille, N., and Bernado, P. (2012). Structural characterization of intrinsically disordered proteins by the combined use of NMR and SAXS. Biochem. Soc. Trans. *40*, 955–962.

Sibille, N., Huvent, I., Fauquant, C., Verdegem, D., Amniai, L., Leroy, A., Wieruszeski, J.-M., Lippens, G., and Landrieu, I. (2012). Structural characterization by nuclear magnetic resonance of the impact of phosphorylation in the proline-rich region of the disordered Tau protein. Proteins *80*, 454–462.

Sillen, A., Barbier, P., Landrieu, I., Lefebvre, S., Wieruszeski, J.M., Leroy, A., Peyrot, V., and Lippens, G. (2007). NMR investigation of the interaction between the neuronal protein tau and the microtubules. Biochemistry *46*, 3055–3064.

Tjandra, N., and Bax, A. (1997). Direct measurement of distances and angles in biomolecules by NMR in a dilute liquid crystalline medium. Science *278*, 1111–1114.

Vuister, G.W., Delaglio, F., and Bax, A. (1993). The use of 1JC alpha H alpha coupling constants as a probe for protein backbone conformation. J. Biomol. NMR *3*, 67–80.

Weingarten, M.D., Lockwood, A.H., Hwo, S.Y., and Kirschner, M.W. (1975). A protein factor essential for microtubule assembly. Proc. Natl. Acad. Sci. USA *72*, 1858–1862.

Wüthrich, K. (1986). NMR of Proteins and Nucleic Acids (Wiley).

Xiang, S., Gapsys, V., Kim, H.-Y., Bessonov, S., Hsiao, H.-H., Möhlmann, S., Klaukien, V., Ficner, R., Becker, S., Urlaub, H., et al. (2013). Phosphorylation drives a dynamic switch in serine/arginine-rich proteins. Structure *21*, 2162–2174.

